Comparison of Sub 6 GHz and mmWave Wireless Channel Measurements at High Speeds

Faruk Pasic*, Daniel Schützenhöfer*†, Edgar Jirousek*†, Robert Langwieser*, Herbert Groll*,
Stefan Pratschner*†, Sebastian Caban*, Stefan Schwarz*†, Markus Rupp*
†Christian Doppler Laboratory for Dependable Wireless Connectivity for the Society in Motion
*Institute of Telecommunications, TU Wien, Austria
faruk.pasic@tuwien.ac.at

***Abstract*—Next-generation mobile communication systems employ millimeter wave (mmWave) frequency bands with high bandwidths to enable high data rate transmissions. Further, the importance of high mobility scenarios, such as vehicular communication or high-speed train scenarios, is steadily increasing. To learn how wave propagation and scattering effects change from classical sub 6 GHz to mmWave frequencies, measurements in both bands have to be conducted. We perform wireless channel measurements at 2.55 GHz and 25.5 GHz center frequency at high mobility. To ensure a fair comparison between these two frequency bands, we perform repeatable measurements in a controlled environment. Our measurement methodology enables measurements at the same transmitter and receiver positions and velocities, but at different center frequencies. We compare measured wireless channels at the two employed frequency bands in terms of the delay-Doppler function.**

***Index Terms*—mmWave, sub 6 GHz, 5G, vehicular communications, high-speed train, testbed, channel measurements.**

I. Introduction

Increasing demand for high data rate transmission in high-speed train (HST) and vehicle-to-everything (V2X) scenarios forces future wireless communication systems towards new transmission technologies. Conventional wireless communication systems operate mostly in sub 6 GHz bands, where they can not keep up with the growing demand for high data rates. On the other hand, millimeter wave (mmWave) bands allow for significantly higher data rates [1], [2].

High-mobility scenarios in sub 6 GHz bands have been well investigated in realistic environments [3]–[9]. Besides sub 6 GHz bands, measurements were also performed at mmWave frequencies in real-world, highly time-variant radio channels [10]–[17]. Several comparisons between sub 6 GHz and mmWave bands have been derived through simulations [18], [19] and measurements [20]. Vehicular multi-band measurements, involving sub 6 GHz and mmWave frequencies, were performed in [21], [22]. The problem here is when using different antennas for different frequency bands, these antennas cannot be placed at the same position at the same time. Placing antennas for different frequency bands several centimeters apart for mechanical reasons means a position offset of several wavelengths at mmWave frequencies. This difference in antenna position may result in a different small-scale fading behavior or altered channel statistics. To compare the wireless channel at the same antenna positions with different antennas at different frequencies, repeatable experiments are required.

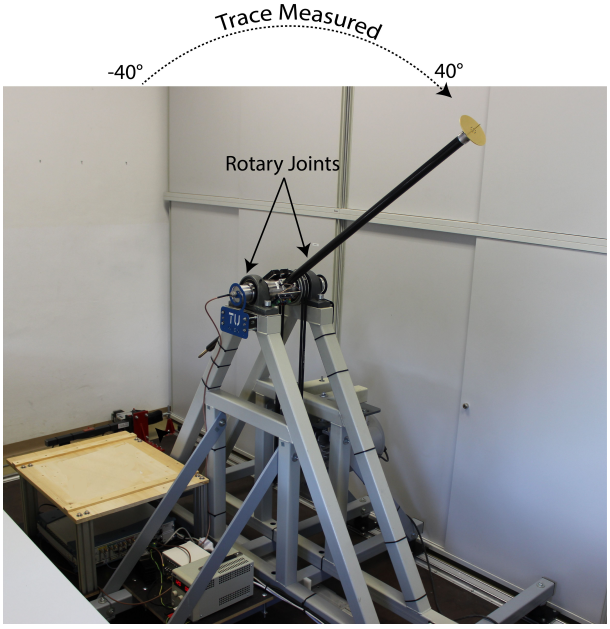

Fig. 1. Measurement setup to compare sub 6 GHz and mmWave in a high-mobility environment. There is either a sub 6 GHz Tx antenna or a mmWave Tx PCB mounted at the end of the rotary arm.

We describe our testbed hardware for sub 6 GHz and mmWave in Section II. The measurement campaign with all measured and compared scenarios is described in Section III. We provide results of the measured wireless channel in terms of the delay-Doppler function in Section IV and conclude our work in Section V.

Contribution: We conduct wireless channel measurements at 2.55 GHz and 25.5 GHz with a moving transmit antenna based on the testbed hardware and the methodology proposed in [23]. Our measurement setup and methodology allow wireless channel measurements from the same transmitter and receiver position, with the same transmitter velocity, but at different frequencies. We select the channel sounding parameters such that the channel measurements are performed for an identical transmit antenna trace for all measured scenarios. As a first result, we compare the measured wireless channel in

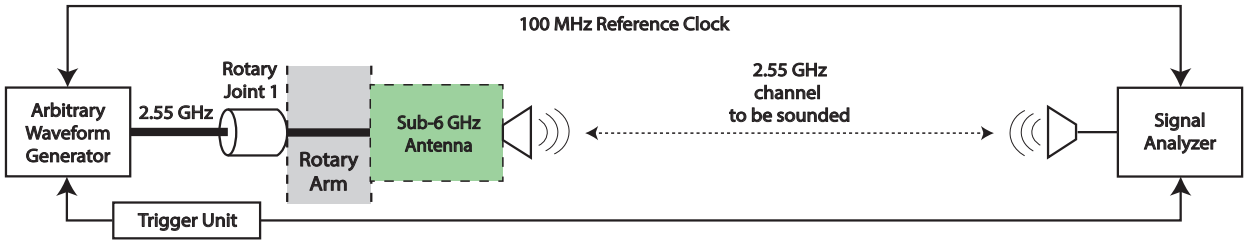

(a) Sub 6GHz setup. The transmit signal is directly generated by the arbitrary waveform generator.

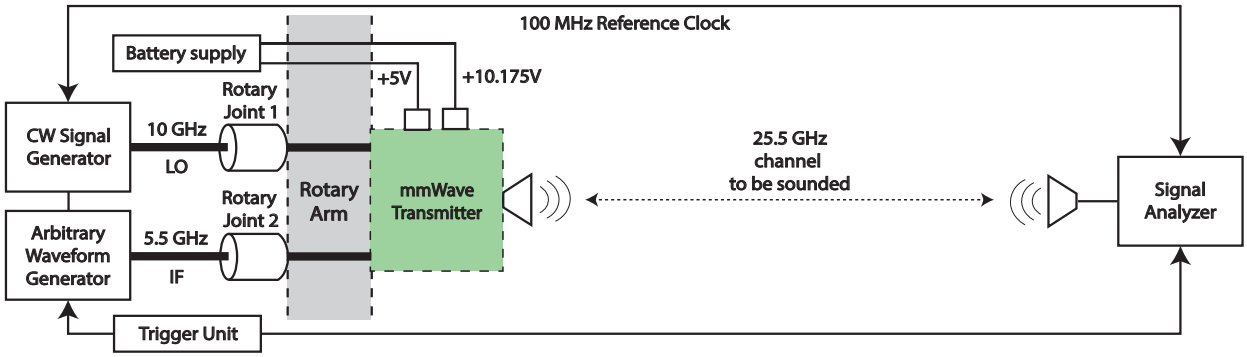

(b) mmWave setup. The transmit signal is generated by the mmWave transmitter from an IF and an LO signal at the end of the rotary arm.

Fig. 2. Channel sounding hardware setup for the sub 6 GHz and the mmWave case.

terms of a delay-Doppler function for the center frequencies of 2.55 GHz and 25.5 GHz.

II. Testbed Architecture

A rotary unit rotates an antenna at the end of a 1 m long arm around a central axis at a constant but adjustable velocity, see Fig. 1. This rotary unit is equipped with a trigger unit, which generates a trigger pulse at an adjustable arm angle, once per revolution. This testbed setup allows repeatable measurements in a controlled environment at high velocities of up to 400 km/h [24], [25]. There are rotary joints at each end of the central axis to feed the radio frequency (RF) signals from a signal source through the rotating arm. These rotary joints have a maximum rotational speed of 1500 rpm and a maximum signal frequency of 12.4 GHz. Therefore, direct transmissions of sub 6 GHz signals with an antenna mounted at the end of the rotating arm are possible. Exploiting the described testbed hardware for mmWave signals, however, requires modifications to the setup.

Modifying the rotary unit to allow direct mmWave band signal transmission requires the replacement of the rotary joints and the rotating arm, including the cables and RF connectors. This straightforward approach leads to two drawbacks: a) the coaxial cables and the rotary joint have high insertion loss at mmWave frequencies and b) rotary joints for mmWave frequencies allow only limited rotational speeds. Therefore, we employ the very common idea of frequency up-conversion from an intermediate frequency (IF) to the mmWave RF frequency very close to the transmit antenna.

At the transmitter side, we employ an arbitrary waveform generator (AWG) (Keysight M8195A) to generate a transmit signal. In either case, we transmit an orthogonal frequency-division multiplexing (OFDM) signal. We chose a Zadoff-Chu sequence as transmit symbols to obtain a transmit signal of low crest factor [26]. At the receiver side, we sample the received signal with a signal analyzer (Rohde & Schwarz FSW67).

A. Sub 6 GHz

In the sub 6 GHz case, the transmit signal is generated with the AWG, directly at a center frequency of 2.55 GHz, see Fig. 2a. The transmit signal is fed through the rotary joint to the monopole antenna at the end of the arm, see Fig. 3a. At the receiver side, we employ a vertical dipole antenna, connected to the signal analyzer, which acts as the receiver.

B. Millimeter Wave

For mmWave frequency signal transmission, we perform a frequency up-conversion by means of a mmWave transmitter at the end of the arm. Due to the high acceleration forces at the end of the spinning arm, this mmWave transmitter hardware needs to be of compact size and light weight. Employing commercially available, bulky, connectorized RF modules is therefore not possible. We developed a mmWave transmitter PCB as described in [23]. This 6-layered PCB with RF dielectric substrate has four coaxial connectors and all surface mount device (SMD) components on the side facing the rotary unit's central axis and a monopole antenna with a ground plane on the other side, see Fig. 3b. The mmWave transmitter mainly consists of an up-converter, a bandpass filter, a power amplifier and the monopole antenna. Please note that the entire mmWave transmitter PCB, as shown in Fig. 3b, has a total weight of only 43.1 g. This is truly a lightweight design compared to the

(a) Sub 6 GHz antenna: connectors (left) and monopole antenna (right).

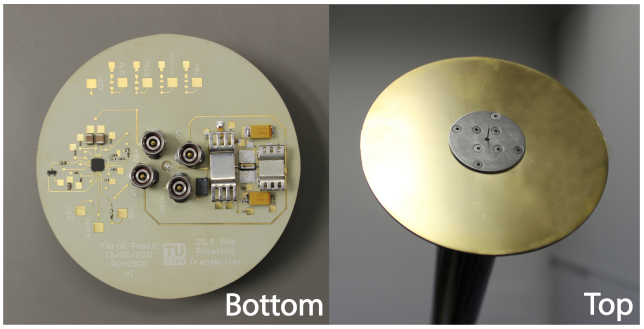

(b) mmWave transmitter: SMD components (left) and monopole antenna (right).

Fig. 3. Employed rotating transmit antennas. The sub 6 GHz antenna is a purely passive monopole while the mmWave antenna consists of the mmWave transmitter and a monopole antenna.

sub 6 GHz antenna, show in Fig. 3a, which has a total weight of 44.3 g.

We utilize one rotary joint for the IF signal and the other rotary joint for the local oscillator (LO) signal, see Fig. 2b. The DC supply of the mmWave transmitter is provided by a battery power supply, mounted on the central rotating axis such that there are only small acceleration forces to this part.

The up-converter performs internal LO frequency doubling which leads to an RF frequency of

$$f_{\mathrm{RF}} = 2f_{\mathrm{LO}} + f_{\mathrm{IF}}. \tag{1}$$

With an LO frequency of f_{LO} =10 GHz and an IF center frequency of f_{IF} =5.5 GHz, we obtain an RF signal with a center frequency of f_{RF} =25.5 GHz.

The signal at IF is again generated with the AWG, the LO is generated by a continuous wave (CW) signal generator and the received signal is sampled by the signal analyzer. For a fair comparison between the sub 6 GHz and the mmWave case, we require a mmWave receive antenna with the same pattern as the sub 6 GHz receive antenna. Unfortunately, in the mmWave case, we need to overcome large path loss that occurs due to the high frequency used. Therefore, we employ a horn antenna with 15 dBi gain as the receive antenna. We assume that our horn antenna with 3-dB opening angle of 30° captures most of the dominant multipath components.

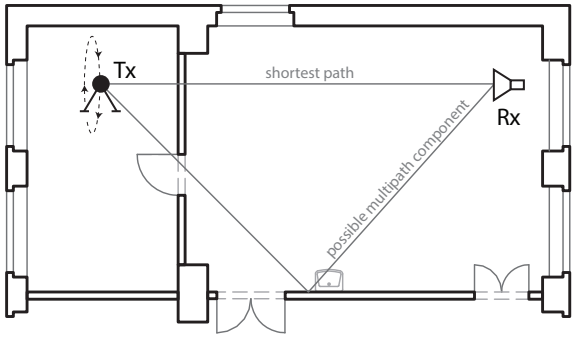

Fig. 4. Measured indoor environment. The receive antenna is located in a rich scattering laboratory environment.

III. Measurement Campaign

We perform wireless channel measurements in a controlled indoor laboratory environment as shown in Fig. 4. We conduct measurements with all four combinations of low (20 km/h) or high (200 km/h) speed and sub 6 GHz (2.55 GHz) or mmWave (25.5 GHz) center frequency, with parameters provided in Fig. 5. The transmit antenna is moving on a circular arc with a constant velocity at the rotary unit and the receive antenna is static on a laboratory table in the neighboring room. For all measured scenarios, the wireless channel is measured with the same transmit antenna positions and the same receive antenna position but with different center frequencies and velocities. This allows a direct comparison of the measured wireless channel in terms of fading environment and channel statistics.

For a direct and fair comparison of the measurement scenarios, the fading environment (the laboratory) has to be static. Therefore, we conduct the measurement campaign within 15 minutes with no people or moving objects within the room during the measurements.

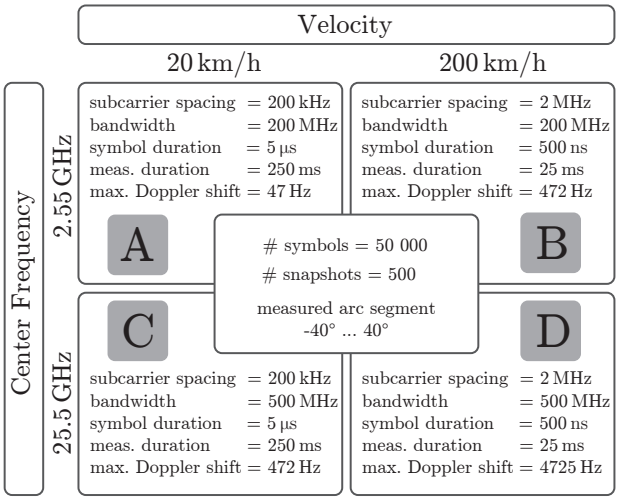

Fig. 5. Measurement parameters for all four measured scenarios. Due to our measurement parametrization, the wireless channel is measured at the same spatial positions for all scenarios.

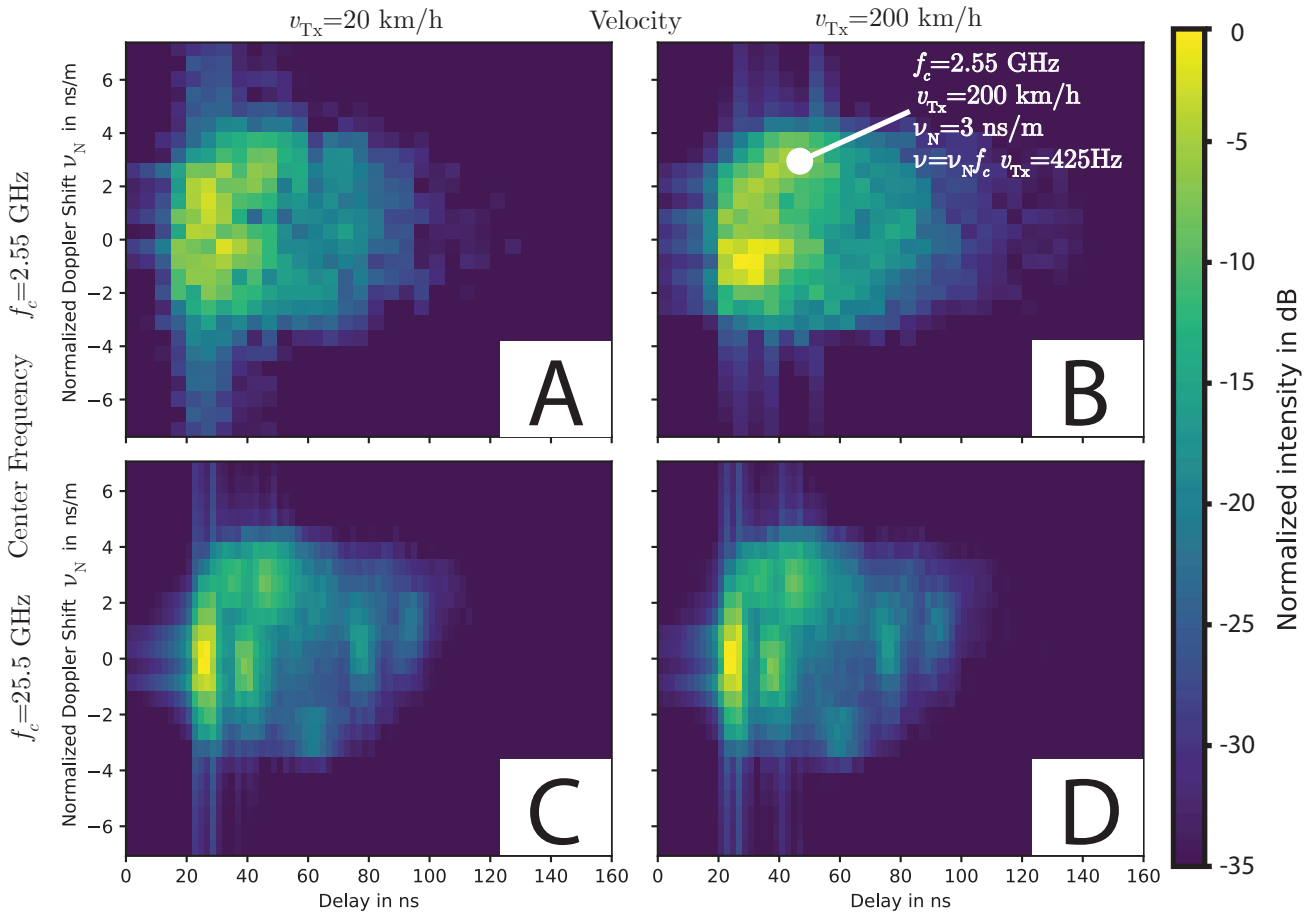

Fig. 6. Measurement results in terms of the delay-Doppler function for different frequency bands and velocities.

We transmit a series of identical OFDM symbols as channel sounding sequence. The transmission is initiated by the trigger unit when the rotating arm is at an angular position of $-40°$. We choose a high subcarrier spacing of 2 MHz for high-velocity measurements and a low subcarrier spacing of 200 kHz for low-velocity measurements. Thereby, we achieve comparability of measurement results, since the rotating antenna moves along the same trace (arc segment) from $-40°$ to $40°$ for all measurement scenarios, see Fig. 1. Please note that the maximum Doppler shift for the Scenario B and the Scenario C are the same, see Fig. 5.

We partition each measurement sequence of 50 000 OFDM symbols into 500 snapshots of 100 symbols each. We assume the wireless channel between the moving antenna and the static receiver to be constant in time for the duration of one snapshot. At the receiver side, we exploit the first OFDM symbol of each snapshot as a cyclic prefix, discard it, and perform averaging of the remaining 99 symbols to improve the signal-to-noise ratio (SNR) by approx. 20 dB. After OFDM processing, we estimate the wireless channel via least-squares estimation for all subcarriers. In this way, we obtain a time-variant channel transfer function for discrete-time (snapshots) and frequency (subcarriers).

IV. Results

Similar as in [21] and [11], we employ the concept from [27] to estimate the mean local scattering function (LSF) of the channel in each of the four scenarios. For each scenario, we proceed as follows: We assume the channel to be locally stationary within a window of approx. six wavelengths of motion and over the entire frequency range, without further justification. A window of six wavelengths corresponds to 250 snapshots for the 2.55 GHz case and 25 snapshots for the 25.5 GHz case. The LSFs of each window are then averaged to produce the average LSFs shown in Fig. 6. We perform two normalizations to ease a comparison of the results: Firstly, we define the normalized Doppler Shift ν_N as

$$\nu_{\mathrm{N}} = \frac{\nu}{f_{\mathrm{c}} v_{\mathrm{Tx}}}, \tag{2}$$

where f_{c} is the center frequency and v_{Tx} is the Tx velocity and ν is the Doppler shift. This way, the supports of the delay-Doppler functions are confined to same interval of ν_{N}. Secondly, the intensity of the normalized Doppler shift is

normalized such that 0 dB is the greatest occurring value in each scenario. The results are shown in Fig. 6. We point out the two key observations:

(i) The normalized delay-Doppler function is invariant with regard to the transmitter's velocity, that is, scenarios A and B look alike, just as C and D.

(ii) The scattering environment is frequency selective, thus resulting in different LSFs for different frequency bands, that is, scenarios A and C look different, just as B and D.

V. Conclusion

We can perform measurements to compare sub 6 GHz and mmWave in high-mobility scenarios. The delay-Doppler functions measured at two different center frequencies look different even when measured on the same trace with the same velocity.

Acknowledgment

This work has been funded by the Christian Doppler Laboratory for Dependable Wireless Connectivity for the Society in Motion. The financial support by the Austrian Federal Ministry for Digital and Economic Affairs, the National Foundation for Research, Technology and Development, and the Christian Doppler Research Association is gratefully acknowledged.

References

[1] B. Ai, A. F. Molisch, M. Rupp, and Z. D. Zhong, "5G key technologies for smart railways," *Proceedings of the IEEE*, vol. 108, no. 6, 2020.

[2] E. Jirousek, Z. Huang, S. Pratschner, R. Langwieser, S. Schwarz, and M. Rupp, "Mmwave fronthaul-to-backhaul interference in 5g nr networks," in *2021 IEEE 32nd Annual International Symposium on Personal, Indoor and Mobile Radio Communications (PIMRC)*, 2021.

[3] F. Kaltenberger, A. Byiringiro, G. Arvanitakis, R. Ghaddab, D. Nussbaum, R. Knopp, M. Bernineau, Y. Cocheril, H. Philippe, and E. Simon, "Broadband wireless channel measurements for high speed trains," in *2015 IEEE International conference on communications (ICC)*.

[4] T. Zhou, C. Tao, and L. Liu, "LTE-assisted multi-link MIMO channel characterization for high-speed train communication systems," *IEEE Transactions on Vehicular Technology*, vol. 68, no. 3, 2018.

[5] J. Yang, B. Ai, S. Salous, K. Guan, D. He, G. Shi, and Z. Zhong, "An efficient MIMO channel model for LTE-R network in high-speed train environment," *IEEE Transactions on Vehicular Technology*, vol. 68, no. 4, pp. 3189–3200, 2019.

[6] D. Schuetzenhoefer, E. Zoechmann, M. Lerch, S. Pratschner, H. Groll, S. Caban, and M. Rupp, "Experimental evaluation of the influence of fast movement on virtual antenna arrays," in *WSA 2019; 23rd International ITG Workshop on Smart Antennas*, 2019, pp. 1–5.

[7] M. Lerch, "Experimental comparison of fast-fading channel interpolation methods for the LTE uplink," in *2015 57th International Symposium ELMAR (ELMAR)*, 2015, pp. 5–8.

[8] R. Nissel, M. Lerch, and M. Rupp, "Experimental validation of the OFDM bit error probability for a moving receive antenna," in *2014 IEEE 80th Vehicular Technology Conference (VTC2014-Fall)*, 2014.

[9] R. Nissel and M. Rupp, "Doubly-selective MMSE channel estimation and ICI mitigation for OFDM systems," in *2015 IEEE International Conference on Communications (ICC)*, 2015, pp. 4692–4697.

[10] E. Zöchmann, M. Hofer, M. Lerch, S. Pratschner, L. Bernadó, J. Blumenstein, S. Caban, S. Sangodoyin, H. Groll, T. Zemen, A. Prokeš, M. Rupp, A. F. Molisch, and C. F. Mecklenbräuker, "Position-specific statistics of 60 GHz vehicular channels during overtaking," *IEEE Access*, vol. 7, pp. 14 216–14 232, 2019.

[11] E. Zöchmann, C. F. Mecklenbräuker, M. Lerch, S. Pratschner, M. Hofer, D. Löschenbrand, J. Blumenstein, S. Sangodoyin, G. Artner, S. Caban, T. Zemen, A. Prokeš, M. Rupp, and A. F. Molisch, "Measured delay and Doppler profiles of overtaking vehicles at 60 GHz," in *12th European Conference on Antennas and Propagation (EuCAP 2018)*, 2018, pp. 1–5.

[12] J. Park, J. Lee, K. Kim, and M. Kim, "28-GHz high-speed train measurements and propagation characteristics analysis," in *2020 14th European Conference on Antennas and Propagation (EuCAP)*, 2020.

[13] D. He, B. Ai, K. Guan, Z. Zhong, B. Hui, J. Kim, H. Chung, and I. Kim, "Channel measurement, simulation, and analysis for high-speed railway communications in 5G millimeter-wave band," *IEEE Transactions on Intelligent Transportation Systems*, vol. 19, no. 10, pp. 3144–3158, 2018.

[14] J. Park, J. Lee, K. Kim, M. Kim, H. Kwon, and K. C. Lee, "Wide-sense stationarity of millimeter wave expressway channels based on 28 GHz measurements," in *2019 IEEE 90th Vehicular Technology Conference (VTC2019-Fall)*, 2019, pp. 1–5.

[15] H. Groll, E. Zöchmann, S. Pratschner, M. Lerch, D. Schützenhöfer, M. Hofer, J. Blumenstein, S. Sangodoyin, T. Zemen, A. Prokeš, A. F. Molisch, and S. Caban, "Sparsity in the delay-doppler domain for measured 60 GHz vehicle-to-infrastructure communication channels," in *2019 IEEE International Conference on Communications Workshops (ICC Workshops)*, 2019, pp. 1–6.

[16] J. Blumenstein, A. Prokes, J. Vychodil, T. Mikulasek, J. Milos, E. Zöchmann, H. Groll, C. F. Mecklenbräuker, M. Hofer, D. Löschenbrand, L. Bernadó, T. Zemen, S. Sangodoyin, and A. Molisch, "Measured high-resolution power-delay profiles of non-stationary vehicular millimeter wave channels," in *2018 IEEE 29th Annual International Symposium on Personal, Indoor and Mobile Radio Communications (PIMRC)*, 2018, pp. 1–5.

[17] G. Yue, D. Yu, L. Cheng, Q. Lv, Z. Luo, Q. Li, J. Luo, and X. He, "Millimeter-wave system for high-speed train communications between train and trackside: System design and channel measurements," *IEEE Transactions on Vehicular Technology*, vol. 68, no. 12, 2019.

[18] M. Giordani, A. Zanella, and M. Zorzi, "LTE and millimeter waves for V2I communications: An end-to-end performance comparison," in *2019 IEEE 89th Vehicular Technology Conference (VTC2019-Spring)*, 2019.

[19] F. Wiffen, L. Sayer, M. Z. Bocus, A. Doufexi, and A. Nix, "Comparison of OTFS and OFDM in ray launched sub-6 GHz and mmWave line-of-sight mobility channels," in *2018 IEEE 29th Annual International Symposium on Personal, Indoor and Mobile Radio Communications (PIMRC)*, 2018, pp. 73–79.

[20] H. Wang, X. Yin, J. Rodríguez-Piñeiro, J. Lee, and M. Kim, "Shadowing and multipath-fading statistics at 2.4 GHz and 39 GHz in vehicle-to-vehicle scenarios," in *2020 14th European Conference on Antennas and Propagation (EuCAP)*, 2020, pp. 1–5.

[21] M. Hofer, D. Löschenbrand, J. Blumenstein, H. Groll, S. Zelenbaba, B. Rainer, L. Bernadó, J. Vychodil, T. Mikulasek, E. Zöchmann, S. Sangodoyin, H. Hammoud, B. Schrenk, R. Langwieser, S. Pratschner, A. Prokes, A. Molisch, C. Mecklenbräuker, and T. Zemen, "Wireless vehicular multiband measurements in centimeterwave and millimeterwave bands," in *32nd Annual International Symposium on Personal, Indoor and Mobile Radio Communications (PIMRC)*, Helsinki, Finland, Sep. 2021. [Online]. Available: http://thomaszemen.org/papers/Hofer21-PIMRC-paper.pdf

[22] D. Dupleich, R. Muller, C. Schneider, S. Skoblikov, J. Luo, M. Boban, G. Del Galdo, and R. Thoma, "Multi-band vehicle to vehicle channel measurements from 6 GHz to 60 GHz at "T" intersection," in *2nd Connected and Automated Vehicles Symposium (CAVS)*, 2019.

[23] F. Pasic, S. Pratschner, R. Langwieser, D. Schützenhöfer, E. Jirousek, H. Groll, S. Caban, and M. Rupp, "Sub 6 GHz versus mmwave measurements in a controlled high-mobility environment," in *25th International ITG Workshop on Smart Antennas (WSA 2021)*, 2021, pp. 1–5, in press. [Online]. Available: https://publik.tuwien.ac.at/files/publik_297773.pdf

[24] S. Caban, J. Rodas, and J. A. García-Naya, "A methodology for repeatable, off-line, closed-loop wireless communication system measurements at very high velocities of up to 560 km/h," in *2011 IEEE International Instrumentation and Measurement Technology Conference*, 2011.

[25] E. Zöchmann, R. Langwieser, S. Caban, M. Lerch, S. Pratschner, R. Nissel, C. Mecklenbräuker, and M. Rupp, "A millimeter wave testbed for repeatable high velocity measurements," in *European Wireless 2017; 23th European Wireless Conference*, 2017, pp. 1–5.

[26] B.-J. Choi, E.-L. Kuan, and L. Hanzo, "Crest-factor study of MC-CDMA and OFDM," in *50th Vehicular Technology Conference*, vol. 1, 1999.

[27] L. Bernadó, T. Zemen, F. Tufvesson, A. F. Molisch, and C. F. Mecklenbräuker, "Delay and Doppler spreads of nonstationary vehicular channels for safety-relevant scenarios," *IEEE Transactions on Vehicular Technology*, vol. 63, no. 1, 2014.